Computation of Separated Flow Using the Space-Marching Conservative Supra-Characteristics Method

David C. Stookesberry* and J. C. Tannehill†
Iowa State University, Ames, Iowa

Steady, hypersonic viscous flows over compression corners with streamwise separation have been computed using the space-marching conservative supra-characteristics method of Lombard. This method permits stable space marching of the parabolized Navier-Stokes equations through large separated flow regions. The present method has been used to compute surface-pressure, heat-transfer, and skin-friction coefficients for two compression corner cases studied experimentally by Holden and Moselle. The computed results compare favorably with previous Navier-Stokes results and experimental data. The present method has also been compared with the conventional Beam-Warming scheme for solving the parabolized Navier-Stokes equations. Comparisons are made for accuracy, computer time, and computer storage.

Introduction

THE parabolized Navier-Stokes (PNS) equations have been used extensively in recent years for steady, supersonic viscous flow computations. The PNS equations are a mixed set of hyperbolic-parabolic equations, that may be numerically integrated by marching in space instead of time. Efficient noniterative, implicit schemes for the PNS equations have been developed by Vigneron et al.[1] and Schiff and Steger.[2]

The PNS equations as derived by Lubard and Helliwell[3] differ from the Navier-Stokes equations in that the streamwise viscous terms are neglected. By retaining and appropriately treating the streamwise pressure gradient term, the PNS equations allow information to be propagated upstream within subsonic regions of the flow. If the flow contains moderate to strong adverse pressure gradients, attempts to compute a solution with this elliptic behavior using a space-marching scheme will result in an exponentially growing solution (departure solution). In these cases, artificial viscosity terms may sometimes be used to maintain stability, but the accuracy of the solution is reduced. In order to propagate the information upstream through subsonic regions, global iteration methods have been used by Rakich,[4] Khosla and Lai,[5] Brown,[6] Rubin and Reddy,[7] and Barnett and Davis.[8] These methods utilize repeated marching of the full set of PNS equations in the streamwise direction. This propagates information upstream one or two grid points per sweep. In order to minimize the number of global sweeps needed, the method of Barnett and Davis utilizes a backward-sweep pressure update procedure. In this way, pressure information is propagated throughout the flowfield during each sweep.

If large adverse pressure gradients are present in the flow, streamwise flow reversal may result. Flow situations such as this are often encountered on high-altitude vehicles such as the Space Shuttle Orbiter.[9] If streamwise separation occurs, the eigenvalues change sign causing unstable behavior in PNS methods. The FLARE approximation,[10] where the streamwise convective term is neglected in the x-momentum equation, is commonly used to maintain stability. For accurate solutions, this approximation is limited to small reverse-flow velocities. In order to compute accurately supersonic flows where eigenvalues of differing sign occur (i.e., subsonic and reverse-flow regions), upwind schemes[11-13] have been developed that difference the equations of motion according to the eigenvalue signs.

Lombard et al.[14,15] proposed the conservative supra-characteristics method (CSCM) for eigenvalue-based differencing. The CSCM method involves using a series of matrix transformations to transfer between the conservative and characteristic representations of the gasdynamic equations. In the characteristic form, the equations can be easily split based on the eigenvalue signs. Accurate shock capturing is provided by the conservative nature of the method. Also, stability is maintained by the upwind differencing without the use of damping terms.

Using the CSCM splitting, a stable space-marching technique (CSCM-S) with pseudotime relaxation was developed by Lombard et al.[16] The eigenvalue split permits the solution to be marched through subsonic and reverse-flow regions. With the ability to sweep in opposite directions, the upstream influence can be propagated throughout the flow more efficiently than with repeated sweeps in the streamwise direction. By using a pseudotime procedure, the CSCM-S scheme requires only a single level of data storage compared to related multiple-level methods for the time-accurate Navier-Stokes equations.

In the present work, the CSCM-S scheme has been used to solve the parabolized Navier-Stokes equations for steady hypersonic flows past 18- and 24-deg compression corners. Both compression corner cases contain extensive separated flow regions. The computed results are compared with results obtained from a PNS code which employs the Beam-Warming scheme in conjunction with the global iteration technique of Rakich. Also, comparisons are made with experimental data and a numerical solution of the complete Navier-Stokes equations.

Governing Equations

The equations describing the planar flow of a Newtonian fluid are the two-dimensional, unsteady Navier-Stokes equations. The equations can be written in nondimensional conservation-law form in Cartesian coordinates as

$$\partial_t q + \partial_x (E - E_v) + \partial_y (F - F_v) = 0 \tag{1}$$

Presented as Paper 86-0564 at the AIAA 24th Aerospace Sciences Meeting, Reno, NV, Jan. 6-9, 1986; received Feb. 3, 1986; revision received Nov. 8, 1986.

*Research Assistant, Department of Aerospace Engineering and Computational Fluid Dynamics Center; presently, Engineer, McDonnell Aircraft Company, St. Louis, MO. Member AIAA.

†Manager, Computational Fluid Dynamics Center, and Professor, Department of Aerospace Engineering. Associate Fellow AIAA.

where

$$q=[\rho,\ \rho u,\ \rho v,\ e_t]^T$$

$$E=[\rho u,\ \rho u^2+p,\ \rho uv,\ (e_t+p)u]^T$$

$$F=[\rho v,\ \rho uv,\ \rho v^2+p,\ (e_t+p)v]^T$$

The viscous terms E_v and F_v are described in Ref. 17. The specific total energy is given by

$$e_t=\rho[e+(u^2+v^2)/2]$$

where

$$e=p/[\rho(\gamma-1)]$$

The equations have been nondimensionalized (dimensional quantities are denoted by a tilde) in the following manner:

$$t=\tilde{t}/(\tilde{L}/\tilde{V}_\infty),\quad x=\tilde{x}/\tilde{L},\quad y=\tilde{y}/\tilde{L}$$

$$u=\tilde{u}/\tilde{V}_\infty,\quad v=\tilde{v}/\tilde{V}_\infty,\quad e=\tilde{e}/\tilde{V}_\infty^2$$

$$\rho=\tilde{\rho}/\tilde{\rho}_\infty,\quad T=\tilde{T}/\tilde{T}_\infty,\quad \mu=\tilde{\mu}/\tilde{\mu}_\infty$$

$$p=\tilde{p}/\tilde{\rho}_\infty\tilde{V}_\infty^2,\quad Re_\infty=\tilde{\rho}_\infty\tilde{V}_\infty\tilde{L}/\tilde{\mu}_\infty,\quad M_\infty=\tilde{V}_\infty/\tilde{c}_\infty$$

where $\tilde{L}$ is the reference length of unity. The coefficient of thermal conductivity has been replaced by assuming a constant Prandtl number and the coefficient of viscosity is calculated using Sutherland's equation

$$\mu=T^{3/2}(1+C)/(T+C)$$

where

$$C=110.4K/\tilde{T}_\infty$$

The system of equations is closed using the perfect gas equation of state written in nondimensional form

$$p=\rho T/\gamma M_\infty^2$$

As an aid in the CSCM formulation, pressure (p) is replaced by volumetric internal energy (P) with the relation

$$p=(\gamma-1)P$$

A general transformation of spatial coordinates

$$\xi=\xi(x,y)\qquad \eta=\eta(x,y)$$

is applied to Eq. (1) so that the equation may be differenced on a uniform computational mesh. The resulting equation in chain-rule conservation-law form is

$$\partial_t q+\xi_x\partial_\xi(E-E_v)+\xi_y\partial_\xi(F-F_v)+\eta_x\partial_\eta(E-E_v)+\eta_y\partial_\eta(F-F_v)=0 \tag{2}$$

Thin-Layer Assumption

The complete Navier-Stokes equations are simplified using the thin-layer assumption in order to reduce computation time and to permit marching of the solution in space when the unsteady terms are omitted. For flows with high Reynolds numbers, the streamwise viscous derivatives are negligible in comparison with the viscous derivatives in the normal direction and are, therefore, not computed. The resulting system of thin-layer equations is

$$\partial_t q+\xi_x\partial_\xi E+\xi_y\partial_\xi F+\eta_x\partial_\eta(E-\tilde{E}_v)+\eta_y\partial_\eta(F-\tilde{F}_v)=0 \tag{3}$$

where $\tilde{E}_v$ and $\tilde{F}_v$ contain no streamwise derivatives.

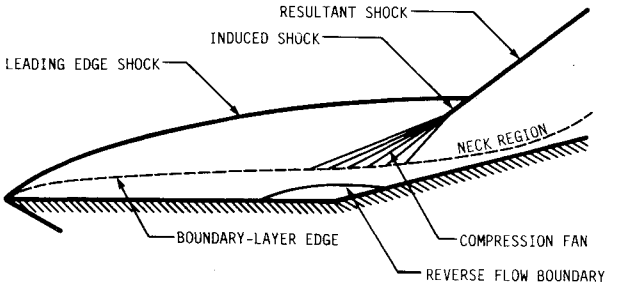

Fig. 1 Hypersonic compression corner case.

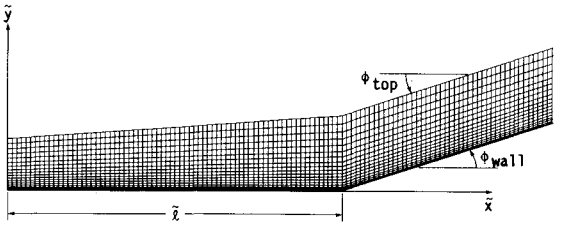

Fig. 2 Physical grid.

Numerical Solution of Equations

CSCM Flux Difference Splitting

The numerical scheme used in the present study is the conservative supra-characteristics methods combined with a space-marching technique (CSCM-S).[14-16] The method is an eigenvalue-based scheme to integrate hyperbolic systems of gasdynamic equations. By adding viscous terms in the normal direction, Lombard et al.[15] demonstrated the capability of the method to solve the PNS equations.

The flux difference vector may be written as a function of the conservative (∂q), nonconservative ($\partial\tilde{q}$), or characteristic ($\partial\tilde{\tilde{q}}$) difference variables.

$$\partial_x E=A\partial_x q=MT\Lambda T^{-1}M^{-1}\partial_x q \tag{4a}$$

$$=MT\Lambda T^{-1}\partial_x\tilde{q}\equiv MA'\partial_x\tilde{q} \tag{4b}$$

$$=MT\Lambda\partial_x\tilde{\tilde{q}} \tag{4c}$$

where

$$\partial q=[\partial\rho,\ \partial\rho u,\ \partial\rho v,\ \partial e_t]^T$$

$$\partial\tilde{q}=[\partial\rho,\ \rho\partial u,\ \rho\partial v,\ \partial P]^T$$

$$\partial\tilde{\tilde{q}}=\begin{bmatrix}\partial\ell n(P^{1/\gamma}/\rho)\\ (1/c)\partial v\\ \partial(u/c)+\partial\ell nP^{1/\gamma}\\ -\partial(u/c)+\partial\ell nP^{1/\gamma}\end{bmatrix}\begin{matrix}\text{, entropy}\\ \text{, normalized tangential velocity}\\ \text{, } P^+ \text{ compatibility}\\ \text{, } P^- \text{ compatibility}\end{matrix}$$

and c is the normalized local speed of sound. The matrix transformation from nonconservative to conservative representation is given by M, and the transformation from characteristic to nonconservative representation is given by T. The diagonal matrix Λ contains the eigenvalues of the

nonconservative system. The relation

$$\Delta ab = \bar{a}\Delta b + \bar{b}\Delta a$$

uses two-point averages and differences to transfer between nonconservative and conservative forms. Similarly, a finite-difference representation of Eq. (4b) in generalized coordinates is

$$\Delta_\xi \hat{E} = \bar{\xi}_x \Delta_\xi E + \bar{\xi}_y \Delta_\xi F = M(\bar{A}' \Delta_\xi \tilde{q}) \tag{5}$$

where

$$M = \begin{bmatrix} 1 & 0 & 0 & 0 \\ \bar{u} & 1 & 0 & 0 \\ \bar{v} & 0 & 1 & 0 \\ \dfrac{\overline{(u^2+v^2)}}{2} & \bar{u} & \bar{v} & 1 \end{bmatrix}$$

The conservative and nonconservative discrete flux difference vectors are

$\Delta_\xi \hat{E} = M(\bar{A}' \Delta_\xi \tilde{q})$	$\bar{A}' \Delta_\xi \tilde{q}$
$\Delta_\xi \rho W_\xi$	$\bar{W}_\xi \Delta_\xi \rho + \bar{\rho} \Delta_\xi W_\xi$
$\Delta_\xi \rho W_\xi u + \bar{\xi}_x \Delta_\xi (\gamma - 1)P$	$\overline{\rho W}_\xi \Delta_\xi u + \bar{\xi}_x \Delta_\xi (\gamma - 1)P$
$\Delta_\xi \rho W_\xi v + \bar{\xi}_y \Delta_\xi (\gamma - 1)P$	$\overline{\rho W}_\xi \Delta_\xi v + \bar{\xi}_y \Delta_\xi (\gamma - 1)P$
$\Delta_\xi W_\xi (\gamma P + \rho(u^2+v^2)/2)$	$\bar{W}_\xi \Delta_\xi P + \overline{\gamma P} \Delta_\xi W_\xi$

where

$$W_\xi = \bar{\xi}_x u + \bar{\xi}_y v$$

A relationship similar to Eqs. (4b) and (4c) and written in finite-difference form is

$$T^{-1} \bar{A}' \Delta_\xi \tilde{q} \cong \bar{\Lambda} T^{-1} \Delta_\xi \tilde{q} \equiv \bar{\Lambda} \Delta_\xi \tilde{\tilde{q}} \tag{6}$$

The matrix transformation to the scaled characteristic system is

$$T^{-1} = \begin{bmatrix} -1/\bar{\rho} & 0 & 0 & 1/\overline{\gamma P} \\ 0 & \bar{\xi}'_y/\bar{\rho}\bar{c} & -\bar{\xi}'_x/\bar{\rho}\bar{c} & 0 \\ 0 & \bar{\xi}'_x/\bar{\rho}\bar{c} & \bar{\xi}'_y/\bar{\rho}\bar{c} & 1/\overline{\gamma P} \\ 0 & -\bar{\xi}'_x/\bar{\rho}\bar{c} & -\bar{\xi}'_y/\bar{\rho}\bar{c} & 1/\overline{\gamma P} \end{bmatrix}$$

where

$$\xi'_x = \xi_x/\xi \qquad \xi = \xi_x^2 + \xi_y^2$$

$$\xi'_y = \xi_y/\xi \qquad \bar{c} = \sqrt{\overline{\gamma P/\rho}}$$

The eigenvalue matrix of the system is

$$\bar{\Lambda} = \begin{bmatrix} \bar{W}_\xi & & & 0 \\ & \bar{W}_\xi & & \\ & & \bar{W}_\xi + \bar{\xi}\bar{c} & \\ 0 & & & \bar{W}_\xi - \bar{\xi}\bar{c} \end{bmatrix}$$

This eigenvalue matrix can be split into positive and negative components using a diagonal matrix of ones and zeros

$$\Lambda = \bar{\Lambda}^+ + \bar{\Lambda}^- = D^+ \bar{\Lambda} + D^- \bar{\Lambda} \tag{7}$$

where

$$D^+ = \frac{1}{2}\left(\frac{\bar{\Lambda}}{|\bar{\Lambda}|} + I\right), \quad D^- = \frac{1}{2}\left(\frac{\bar{\Lambda}}{|\bar{\Lambda}|} - I\right)$$

In a similar fashion, Eq. (6) can be split as

$$T^{-1} \bar{A}' \Delta_\xi \tilde{q} = D^+ T^{-1} \bar{A}' \Delta_\xi \tilde{q} + D^- T^{-1} \bar{A}' \Delta_\xi \tilde{q} = \bar{\Lambda} \Delta_\xi \tilde{\tilde{q}}$$

The conservative flux difference split is obtained by the sequence of transformations to the nonconservative and conservative representation

$$\Delta_\xi \hat{E} = \Delta_\xi \hat{E}^+ + \Delta_\xi \hat{E}^- = MTD^+ T^{-1} \bar{A}' \Delta_\xi \tilde{q} + MTD^- T^{-1} \bar{A}' \Delta_\xi \tilde{q} \tag{8}$$

To complete the flux difference formulation, the nonconservative flux difference is written as a function of the conservative difference variable by the relation

$$\bar{A}' \Delta_\xi \tilde{q} \equiv \tilde{M}^{-1}(\Delta_\xi) q$$

so that

$$\Delta_\xi \hat{E}^+ = MTD^+ T^{-1} \tilde{M}^{-1} \Delta_\xi q \equiv A^+ \Delta_\xi q$$

$$\Delta_\xi \hat{E}^- = MTD^- T^{-1} \tilde{M}^{-1} \Delta_\xi q \equiv A^- \Delta_\xi q \tag{9}$$

The matrices T, M^{-1}, and $\tilde{M}^{-1}$ are given in the Appendix. The CSCM splitting is also used for the flux vector in the η direction

$$\Delta_\eta \hat{F}^+ = B^+ \Delta_\eta q, \qquad \Delta_\eta \hat{F}^- = B^- \Delta_\eta q \tag{10}$$

Finite-Difference Scheme

By adding the flux difference pieces that are propagating toward the mesh point (i,j), the inviscid vector equation is

$$[I + (A^+ \Delta_\xi)_{i-1} + (A^- \Delta_\xi)_i + (B^+ \Delta_\eta)_{j-1} + (B^- \Delta_\eta)_j] \delta q_{i,j}$$
$$= -(A^+ \Delta_\xi q)_{i-1} - (A^- \Delta_\xi q)_i - (B^+ \Delta_\eta q)_{j-1} - (B^- \Delta_\eta q)_j \tag{11}$$

The i and j subscripts denote the beginning of the two-point interval in which the averages and differences are computed. The time increment (δt) is absorbed into the A and B matrices.

The CSCM implicit upwind scheme is used to construct a stable space-marching (CSCM-S) method. Using the asterisk superscript to denote an intermediate time, the one-dimensional vector equation similar to Eq. (11) is

$$\delta q_i^* + A_{i-1}^+ (\delta q_i^* - \delta q_{i-1}^*) + A_i^- (\delta q_{i+1}^* - \delta q_i^*)$$
$$= -A_{i-1}^+ (q_i^n - q_{i-1}^n) - A_i^- (q_{i+1}^n - q_i^n) \tag{12}$$

where

$$\delta q_i^* = q_i^* - q_i^n$$

For a forward-marching sweep, two substitutions are made for the solution procedure at mesh point (i):

$$\delta q_{i-1}^* = q_{i-1}^* - q_{i-1}^n$$

$$\delta q_{i+1}^* = 0$$

The resulting forward-sweep equation is

$$(I + A_{i-1}^+ - A_i^-) \delta q_i^* = -A_{i-1}^+ (q_i^n - q_{i-1}^*) - (A^- \Delta_\xi q)_i^n \tag{13}$$

An equation similar to Eq. (13) can be written for the backward-marching sweep

$$(I+A_{i-1}^{+}-A_{i}^{-})\delta q_{i}^{n+1}=-(A^{+}\Delta_{\xi}q)_{i-1}^{*}-A_{i}^{-}(q_{i+1}^{n+1}-q_{i}^{*}) \quad (14)$$

Note that the characteristic waves running in the same direction as the marching sweep are propagated throughout the flow, while the waves running in the opposite direction are only propagated locally.

The inviscid forward-sweep equation in two dimensions is

$$(I+A_{i-1}^{+}-A_{i}^{-}+B_{j-1}^{+}\nabla_{\eta}+B_{j}^{-}\Delta_{\eta})\delta q_{i,j}^{*}=-A_{i-1}^{+}(q_{i}^{n}-q_{i-1}^{*})$$
$$-(A^{-}\Delta_{\xi}q)_{i}-(B^{+}\Delta_{\eta}q)_{j-1}-(B^{-}\Delta_{\eta}q)_{j} \quad (15)$$

and likewise for the backward-sweep equation. To complete the thin-layer formulation, centrally differenced viscous terms, similar to those given by Steger,[18] are added in the η direction. As the equations are marched forward and backward, the variables are updated along a $\xi=$const line using a block tridiagonal solver. At each streamwise station, the solution procedure is iterated several times in order to make the coefficient matrices consistent with the new time step. A spatially varying time step, as described by Coakley,[19] is used to accelerate convergence to steady state. Time accuracy is lost when the space-marching method is used, but the storage requirement is reduced to a single level for the flowfield. For strictly supersonic flow, the solution can be obtained in one marching sweep. A converged solution can be computed at each streamwise station in succession, similar to traditional space-marching PNS techniques.

To increase accuracy, three-point differencing is used for the inviscid terms on the right-hand side of the equation. In one dimension, the resulting second-order method is

$$(I+A_{i-1}^{+}-A_{i}^{-})\delta q_{i}=[-3(A^{+}\Delta_{\xi}q)_{i-1}$$
$$+(A^{+}\Delta_{\xi}q)_{i-2}-3(A^{-}\Delta_{\xi}q)_{i}+(A^{-}\Delta_{\xi}q)_{i+1}]/2 \quad (16)$$

A switching procedure discussed in Ref. 16 is used to prevent oscillations caused by differencing with higher-order methods across eigenvalue sign changes. The procedure switches to first-order differencing along subsonic and reverse flow boundaries.

Computational Grid

When viscous effects are being computed, it is necessary to cluster grid points within the viscous layer to produce accurate results. In the present study, this was accomplished using the Roberts clustering function[10]

$$z(\eta)=\frac{\beta+1-(\beta-1)[(\beta+1)/(\beta-1)]^{1-\eta}}{[(\beta+1)/(\beta-1)]^{1-\eta}+1}$$

where $z(\eta)$ is equal to 1 when $\eta=1$ and is 0 when $\eta=0$. The points become more tightly clustered as β approaches 1. The physical distance y can be obtained from

$$y(\xi,\eta)=y_{0}(\xi)+h(\xi)z(\eta)$$

where $y_0(\xi)$ is the height of the wall and $h(\xi)$ is the distance between the top of the grid and the wall. The grid transformation used was

$$\xi=x, \quad \eta=\eta(x,y)$$

The metrics were computed numerically using the following relations:

$$J=1/y_{\eta}, \quad \xi_{x}=1, \quad \xi_{y}=0, \quad \eta_{x}=-Jy_{\xi}, \quad \eta_{y}=J$$

Boundary Conditions

Freestream conditions were imposed along the inflow boundary. Along the top freestream boundary, a zero-gradient condition was implicitly applied. At the outflow boundary, a simple two-point extrapolation was used. Since most of the flow is supersonic and the boundary layer is parabolic at that point, it is assumed that any error propagated upstream from the outflow boundary would be negligible. At the wall boundary, no-slip and constant-temperature boundary conditions were applied.

The CSCM split allows the wall boundary conditions to be substituted for the characteristic relations propagating toward the boundary from outside of the computational domain. The wall boundary condition matrix $\tilde{\tilde{B}}$ is added to the η-direction vector equation so that

$$(\tilde{\tilde{B}}^{-}+B^{-}\Delta_{\eta})_{1}\delta q_{1}=-(B^{-}\Delta_{\eta}q)_{1}$$

For the two-dimensional inviscid equation, the wall boundary condition matrix is applied in the following manner:

$$(I+A_{i-1}^{+}-A_{i}^{-}+(\tilde{\tilde{B}}_{1}^{-})^{-1}B_{1}^{-}\Delta_{\eta})\delta q_{i,1}$$
$$=-[(\tilde{\tilde{B}}^{-})^{-1}B^{-}\Delta_{\eta}q]_{1}-(A^{+}\Delta_{\xi}q)_{i-1}-(A^{-}\Delta_{\xi}q)_{i} \quad (17)$$

The boundary condition matrix is formed by combining the characteristic and boundary condition relations.

$$\tilde{\tilde{B}}^{-}=MT(D^{-}T^{-1}+D^{+}T'^{-1})M^{-1}$$

At the wall, the first three rows of T^{-1} must be replaced. For row 1, constant temperature is maintained by substituting the polytrope law for an isothermal wall.

$$p\sim\rho$$

For rows 2 and 3, the normal and tangential velocities are maintained at zero. The first three rows of T'^{-1} in scaled form are

$$\begin{bmatrix} -1/\rho & 0 & 0 & 1/P \\ 0 & \eta_{y}'/\rho c & -\eta_{x}'/\rho c & 0 \\ 0 & \eta_{x}'/\rho c & -\eta_{y}'/\rho c & 0 \end{bmatrix}$$

The boundary condition procedure is described further in Ref. 14.

Numerical Results

The hypersonic laminar flow over a compression corner was computed. The problem is illustrated in Fig. 1. The flow conditions were chosen to correspond with two of the cases studied experimentally by Holden and Moselle[20] and numerically by Hung and MacCormack[21] using the complete Navier-Stokes equations. The flow conditions were

$$M_{\infty}=14.1, \quad Pr=0.72, \quad \tilde{T}_{\infty}=72.2\ \text{K}, \quad \tilde{T}_{w}=297\ \text{K}$$

$$Re_{\tilde{\ell}}=1.04\times10^{5}, \quad \tilde{\ell}=0.439\ \text{m}, \quad \gamma=1.4$$

The Reynolds number, $Re_{\tilde{\ell}}$, is the freestream Reynolds number based on the distance from the leading edge to the beginning of the ramp. Ramp angles of 18 and 24 deg were used. In both cases, extensive regions of separated flow were present.

The grid used in the calculation is shown in Fig. 2 with every other grid line omitted. Thirty grid points were spaced in the y direction above the wall with a stretching parameter, β, of 1.08. The physical grid had an initial height of $0.148\,\ell$

and the top of the grid was initially at an angle, ϕ_{top}, of 4 deg with respect to horizontal. At the beginning of the ramp, ϕ_{top} changed to either 18 or 24 deg to follow the rise of the wall. Initially, throughout the flowfield, freestream conditions were applied. A constant step size of $\Delta\tilde{x}=3.048\times10^{-3}$ m was used with 236 grid points in the streamwise direction.

Computed wall pressures for the 18-deg-ramp case are shown in Fig. 3. The present results are compared with results obtained using the Beam-Warming scheme[22] to solve the PNS equations, the Navier-Stokes results of Hung and MacCormack,[21] and the experimental results of Holden and Moselle.[20] The wall pressure coefficient is defined by

$$C_p=\tilde{p}_w/\tilde{\rho}_\infty\tilde{V}_\infty^2$$

The results obtained using the Beam-Warming scheme are shown for the conventional single-sweep method and for the global iteration method of Rakich.[4] The CSCM upwind method allows considerably more upstream influence than the global iteration Beam-Warming scheme. The present results and the Navier-Stokes results compared well with the experimental data. The intersection of the leading-edge shock with the wedge-induced shock results in a Type VI interference pattern as classified by Edney.[23] The interference produces an expansion fan, which impinges on the wedge surface near the outflow boundary of the computational domain for the 18-deg-ramp case.

Figure 4 shows a comparison of heat-transfer coefficients as calculated from

$$C_H=\frac{\mu_w}{PrRe_\infty}\frac{\sec(\phi_{wall})}{(\gamma-1/2)M_\infty^2+1-T_w}\frac{\partial T}{\partial y}$$

The present results and Navier-Stokes results are in much better agreement with the experimental data than the conventional PNS results, especially near the ramp leading edge. It is noted that the point of minimum heat transfer is displaced closer to the edge of the ramp for the numerical methods.

Skin-friction coefficients as calculated from

$$C_f=\sec(\phi_{wall})\frac{\mu_w}{Re_\infty}\frac{\partial u}{\partial y}$$

are plotted in Fig. 5. The lack of significant upstream influence in the conventional PNS method greatly decreases the ability to compute reverse-flow regions compared to the present method. The present results and those of Hung and MacCormack compare reasonably well, especially near the points of flow separation and reattachment. The cause of the difference in skin-friction values near the expansion fan impingement area may be due to the absence of streamwise viscous terms in the present method. In this area of the ramp, the velocity near the wall is changing rapidly in the direction tangent to the wall.

As the boundary layer decreases in height behind the ramp leading edge (see Fig. 1), a loss of information occurs along the sonic line. The eigenvalue sign switch that occurs at the sonic line causes information on either side of the sonic line to be propagated away from the grid point. An averaging procedure described in Ref. 16 allows for continuous differencing through the sonic point. The procedure averages the matrices on either side of the sonic point. One-half of the signal that was propagating away from the sonic point is sent toward the point. The method is

$$(I+\bar{A}_i^+ + \bar{A}_i^-)\delta q_i=-\bar{A}_i^+\Delta q_{i-1}-\bar{A}_i^-\Delta q_i \qquad (18)$$

where

$$\bar{A}_i^+=(A_{i-1}^+ + A_i^+)/2, \quad \bar{A}_i^-=(A_{i-1}^- + A_i^-)/2$$

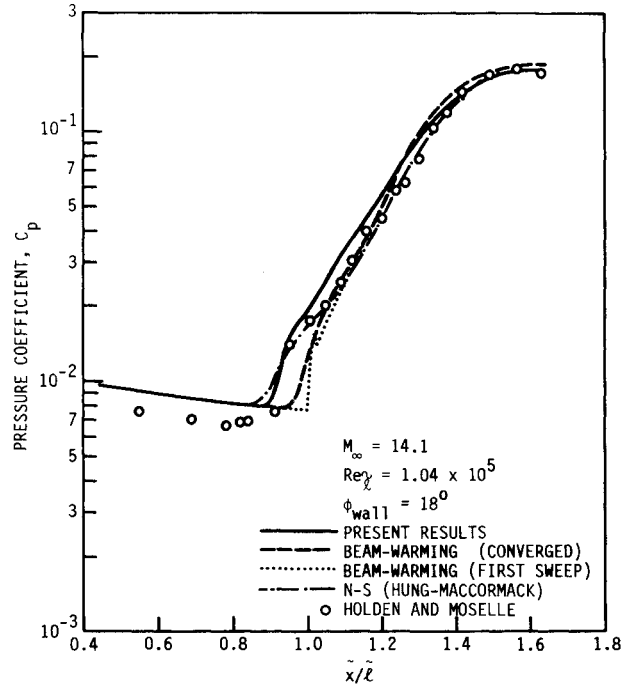

Fig. 3 Comparison of wall-pressure coefficients for an 18-deg ramp.

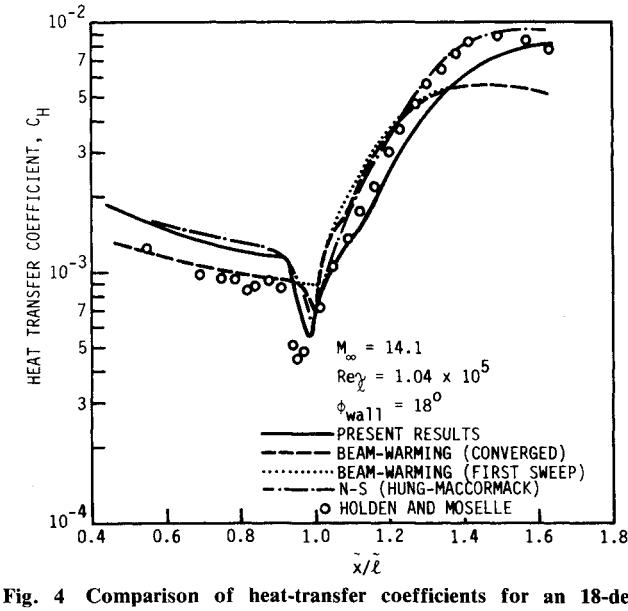

Fig. 4 Comparison of heat-transfer coefficients for an 18-deg ramp.

A similar situation occurs along the reverse-flow boundary near the reattachment point.

A comparison of pressure coefficients for the 24-deg ramp is shown in Fig. 6. The present results are shown along with the results of Hung and MacCormack and the experimental results of Holden and Moselle. A converged solution using the Beam-Warming scheme could not be computed because of stability problems associated with the large region of reverse flow. The numerical results shown agree reasonably well with one another and with the experimental results. The present upwind results show the large area of upstream influence generated by the pressure gradient. The point of peak wall pressure is predicted fairly accurately by both numerical methods when compared to the experimental results.

Figures 7 and 8 compare results for heat-transfer and skin-friction coefficients, respectively. The present solution agrees

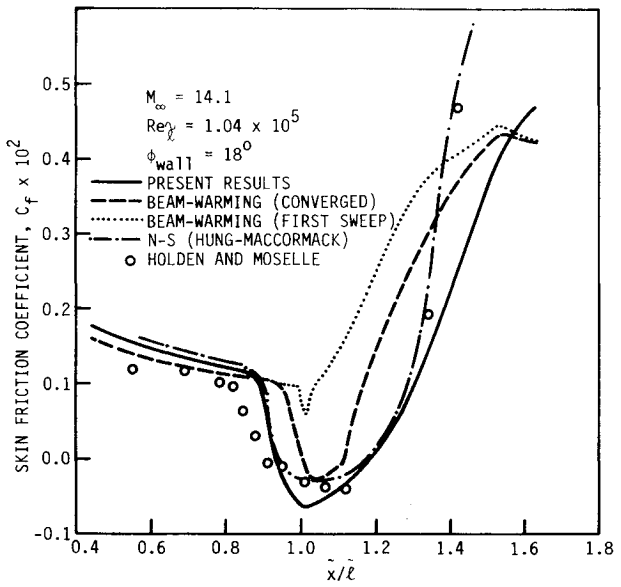

Fig. 5 Comparison of skin-friction coefficients for an 18-deg ramp.

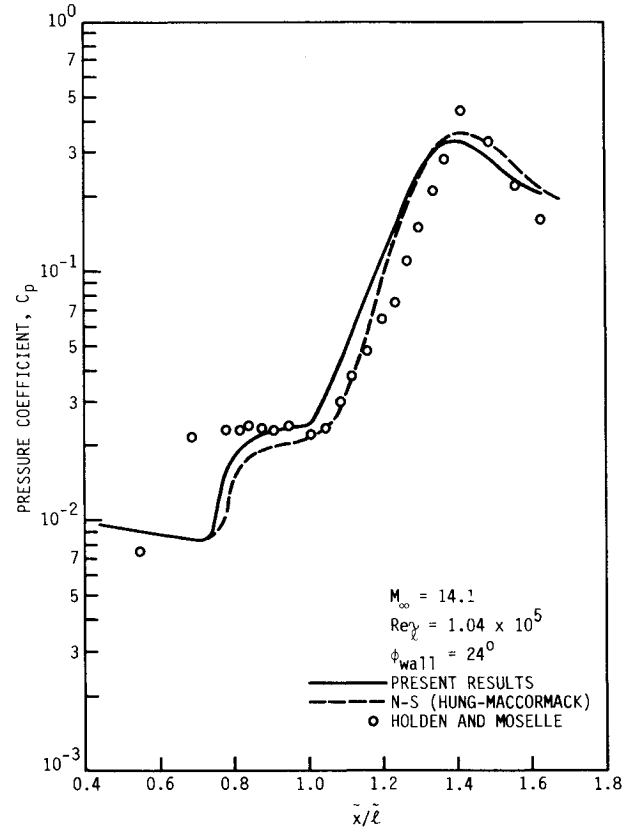

Fig. 6 Comparison of wall-pressure coefficients for a 24-deg ramp.

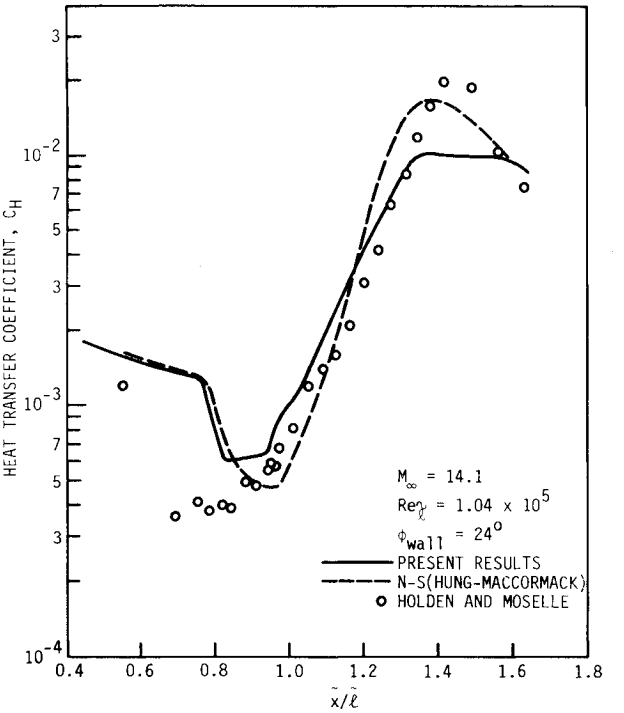

Fig. 7 Comparison of heat-transfer coefficients for a 24-deg ramp.

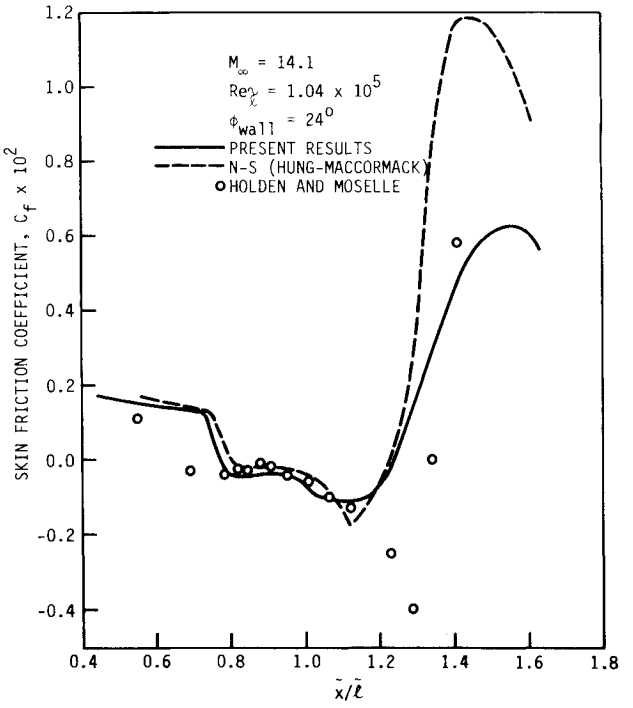

Fig. 8 Comparison of skin-friction coefficients for a 24-deg ramp.

reasonably well with the solution of Hung and MacCormack except in the expansion fan region. The discrepancy in the solution near the expansion fan impingement point is more noticeable than in the 18-deg-ramp case.

For both ramp cases, the second-order CSCM-S method was used. A nonconverged first-order solution was computed and then used to start the second-order method. Along the leading-edge shock, the dispersive nature of the second-order method led to severe overshoot and loss of stability. For this reason, a switch to first-order differencing at the shock was used. The CSCM-S code contained approximately 50% more FORTRAN source lines than the Beam-Warming code primarily because of the CSCM flux difference splitting procedure. The same block tridiagonal solver was used in both codes.

To check for convergence, the rms pressure change for the flowfield was monitored. For the present results, convergence was obtained in ten global sweeps with three inner iterations at each marching step. The converged solution required 8.51×10^{-1} s/grid point of CPU time on a Concurrent (Perkin-Elmer) 3242 computer. A CFL number near unity was used for the initial marching sweeps. The CFL number was then increased to accelerate convergence. The converged Beam-Waming solution utilized 18 streamwise

sweeps and 1.10×10^{-1} s/grid point of CPU time on a Concurrent 3242 computer. To compute the complete Navier-Stokes solution of Hung and MacCormack, 7.11×10^{-1} s/grid point of CPU time on a CDC 7600 computer was required.

While the CSCM-S method requires substantially more CPU time than the Beam-Warming scheme, the ability to compute flows accurately with large pressure gradients and reverse flow may be equally important. The use of the CSCM-S method in conjunction with conventional PNS methods would appear to be very feasible since the CSCM-S method requires only one level of data storage. The most efficient and accurate method could then be used in a particular flow region.

Concluding Remarks

The space-marching conservative supra-characteristics method has been applied to the two-dimensional, parabolized Navier-Stokes equations in order to compute steady supersonic flowfields. The hypersonic laminar flows over 18- and 24-deg compression corners were computed. Both ramp angles resulted in large pressure gradients and extensive areas of reverse flow. The present results compare well with previously published numerical results and experimental data. A comparison was also made with the conventional Beam-Warming PNS scheme, which used single-sweep and global iteration procedures. The present upwind method was more accurate and propagated the upstream influence a much greater distance then the Beam-Warming scheme, but required substantially more computer time.

Appendix

The matrix transformation from the characteristic flux representation to the nonconservative representation is

$$T=\begin{bmatrix} -\bar{\rho} & 0 & \bar{\rho}/2 & \bar{\rho}/2 \\ 0 & \bar{\xi}_y\bar{\rho}\bar{c} & \bar{\xi}_x\bar{\rho}\bar{c}/2 & -\bar{\xi}_x\bar{\rho}\bar{c}/2 \\ 0 & -\bar{\xi}_x\bar{\rho}\bar{c} & \bar{\xi}_y\bar{\rho}\bar{c}/2 & -\bar{\xi}_y\bar{\rho}\bar{c}/2 \\ 0 & 0 & \overline{\gamma P}/2 & \overline{\gamma P}/2 \end{bmatrix}$$

The transformation from the conservative to nonconservative representation is given by

$$M^{-1}=\begin{bmatrix} 1 & 0 & 0 & 0 \\ -\bar{u} & 1 & 0 & 0 \\ -\bar{v} & 0 & 1 & 0 \\ \bar{s}^2-\tfrac{1}{2}\overline{s^2} & -\bar{u} & -\bar{v} & 1 \end{bmatrix}$$

where

$$\bar{s}^2=\bar{u}^2+\bar{v}^2, \quad \overline{s^2}=\overline{u^2}+\overline{v^2}$$

The nonconservative flux vector written as a matrix function of the conservative variable vector q is

$$\tilde{M}^{-1}(\Delta_\xi)=\begin{bmatrix} 0 & m_{12} & m_{13} & 0 \\ m_{21} & m_{22} & m_{23} & m_{24} \\ m_{31} & m_{32} & m_{33} & m_{34} \\ m_{41} & m_{42} & m_{43} & m_{44} \end{bmatrix}$$

where

$$m_{12}=\bar{\xi}_x\Delta_\xi, \quad m_{13}=\bar{\xi}_y\Delta_\xi$$

$$m_{21}=[-\bar{u}\overline{\rho W}_\xi+\bar{\xi}_x\overline{(\gamma-1)\rho s^2}]\frac{1}{\bar{\rho}}\Delta_\xi-\bar{\xi}_x\frac{\overline{s^2}}{2}\Delta_\xi(\gamma-1)$$

$$m_{22}=[\overline{\rho W}_\xi-\xi_x\overline{(\gamma-1)\rho u}]\frac{1}{\bar{\rho}}\Delta_\xi$$

$$m_{23}=-\bar{\xi}_x\overline{(\gamma-1)\rho v}\frac{1}{\bar{\rho}}\Delta_\xi, \quad m_{24}=\bar{\xi}_x\Delta_\xi(\gamma-1)$$

$$m_{31}=[-\bar{v}\overline{\rho W}_\xi+\bar{\xi}_y\overline{(\gamma-1)\rho s^{-2}}]\frac{1}{\bar{\rho}}\Delta_\xi-\bar{\xi}_y\frac{\overline{s^2}}{2}\Delta_\xi(\gamma-1)$$

$$m_{32}=-\bar{\xi}_y\overline{(\gamma-1)\rho u}\frac{1}{\bar{\rho}}\Delta_\xi$$

$$m_{33}=[\overline{\rho W}_\xi-\bar{\xi}_y\overline{(\gamma-1)\rho v}]\frac{1}{\bar{\rho}}\Delta_\xi$$

$$m_{34}=\bar{\xi}_y\Delta_\xi(\gamma-1), \quad m_{41}=(\bar{s}^2-\overline{s^2}/2-\overline{\gamma P/\rho})\bar{W}_\xi\Delta_\xi$$

$$m_{42}=(-\bar{W}_\xi\bar{u}+\bar{\xi}_x\overline{\gamma P/\rho})\Delta_\xi, \quad m_{43}=(-\bar{W}_\xi\bar{v}+\bar{\xi}_y\overline{\gamma P/\rho})\Delta_\xi$$

$$m_{44}=\bar{W}_\xi\Delta_\xi$$

Acknowledgments

This work was supported by NASA Ames Research Center under Grants NGR 16-002-038 and NAG-2-245 (J. G. Marvin, Technical Monitor) and the Computational Fluid Dynamics Center, Iowa State University, Ames, IA.

References

[1]Vigneron, Y. C., Rakich, J. V., and Tannehill, J. C., "Calculation of Supersonic Viscous Flow Over Delta Wings with Sharp Subsonic Leading Edges," AIAA Paper 78-1137, July 1978.

[2]Schiff, L. B. and Steger, J. L., "Numerical Simulation of Steady Supersonic Viscous Flow," AIAA Paper 79-1030, Jan. 1979.

[3]Lubard, S. C. and Helliwell, W. S., "Calculation of the Flow on a Cone at High Angle of Attack," *AIAA Journal*, Vol. 12, July 1974, pp. 965-974.

[4]Rakich, J. V., "Iterative PNS Method for Attached Flows with Upstream Influence," AIAA Paper 83-1955, July 1983.

[5]Khosla, P. K. and Lai, H. I., "Global PNS Solutions for Transonic Strong Interaction Flows," AIAA Paper 84-0458, Jan. 1984.

[6]Brown, J. L., "Parabolized Navier-Stokes Solutions of Separation and Trailing-Edge Flows," NASA TM 84378, June 1983.

[7]Rubin, S. G. and Reddy, D. R., "Global PNS Solutions for Laminar and Turbulent Flow," AIAA Paper 83-1911, July 1983.

[8]Barnett, M. and Davis, R. T., "A Procedure for the Calculation of Supersonic Flows with Strong Viscous-Inviscid Interaction," AIAA Paper 85-0166, Jan. 1985.

[9]Chaussee, D. S. and Rizk, Y. M., "Computation of Viscous Hypersonic Flow Over Control Surfaces," AIAA Paper 82-0291, Jan. 1982.

[10]Anderson, D. S., Tannehill, J. C., and Pletcher, R. H., *Computational Fluid Mechanics and Heat Transfer*, Hemisphere, New York, 1984.

[11]Steger, J. L. and Warming, R. F., "Flux Vector Splitting of the Inviscid Gasdynamic Equations with Application to Finite Difference Methods," NASA TM 78605, July 1979.

[12]Chakravarthy, S. R. and Osher, S., "Numerical Experiments with the Osher Upwind Scheme for the Euler Equations," *AIAA Journal*, Vol. 21, Sept. 1983, pp. 1241-1248.

[13]Chakravarthy, S. R., Anderson, D. A., and Salas, M. D., "The Split-Coefficient Matrix Method for Hyperbolic Systems of Gas Dynamic Equations," AIAA Paper 80-0268, Jan. 1980.

[14]Lombard, C. K., Oliger, J., Yang, J. Y., and Davy, W. C., "Conservative Supra-Characteristics Method for Splitting the

Hyperbolic Systems of Gas Dynamics with Computed Boundaries for Real and Perfect Gases," AIAA Paper 82-0837, June 1982.

[15]Lombard, C. K., Bardina, J., and Venkatapathy, E., "Multi-Dimensional Formulation of CSCM—An Upwind Flux Difference Eigenvector Split Method for the Compressible Navier-Stokes Equations," AIAA Paper 83-1895, July 1983.

[16]Lombard, C. K., Venkatapathy, E., and Bardina, J., "Universal Single Level Implicit Algorithm for Gasdynamics," AIAA Paper 84-1533, June 1984.

[17]Stookesberry, D. C. and Tannehill, J. C., "Computation of Separated Flow on a Ramp Using the Space Marching Conservative Supra-Characteristics Method," AIAA Paper 86-0564, Jan. 1986.

[18]Steger, J. L., "Implicit Finite Difference Simulation of Flow About Arbitrary Geometries with Application to Airfoils," AIAA Paper 77-665, June 1977.

[19]Coakley, T. J., "Numerical Method for Gas Dynamics Combining Characteristic and Conservative Concepts," AIAA Paper 81-1257, June 1981.

[20]Holden, M. S. and Moselle, J. R., "Theoretical and Experimental Studies of the Shock Wave-Boundary Layer Interaction on Compression Surfaces in Hypersonic Flow," CALSPAN Rept. AF-2410-A-1, Buffalo, NY, Oct. 1969.

[21]Hung, C. M. and MacCormack, R. W., "Numerical Solutions of Supersonic and Hypersonic Laminar Compression Corner Flows," *AIAA Journal*, Vol. 14, April 1976, pp. 475-481.

[22]Lawrence, S. L., Tannehill, J. C., and Chaussee, D. S., "Application of the Implicit MacCormack Scheme to the Parabolized Navier-Stokes Equations," *AIAA Journal*, Vol. 22, Dec. 1984, pp. 1755-1763.

[23]Edney, B., "Anomalous Heat-Transfer and Pressure Distributions on Blunt Bodies at Hypersonic Speeds in the Presence of an Impinging Shock," Aeronautical Research Institute of Sweden, Bromma, FAA Rept. 116, Feb. 1968.